The optical layout of the ASTRI prototype: 4 meter Schwarzschild-Couder Cherenkov telescope for CTA with 10° of field of view

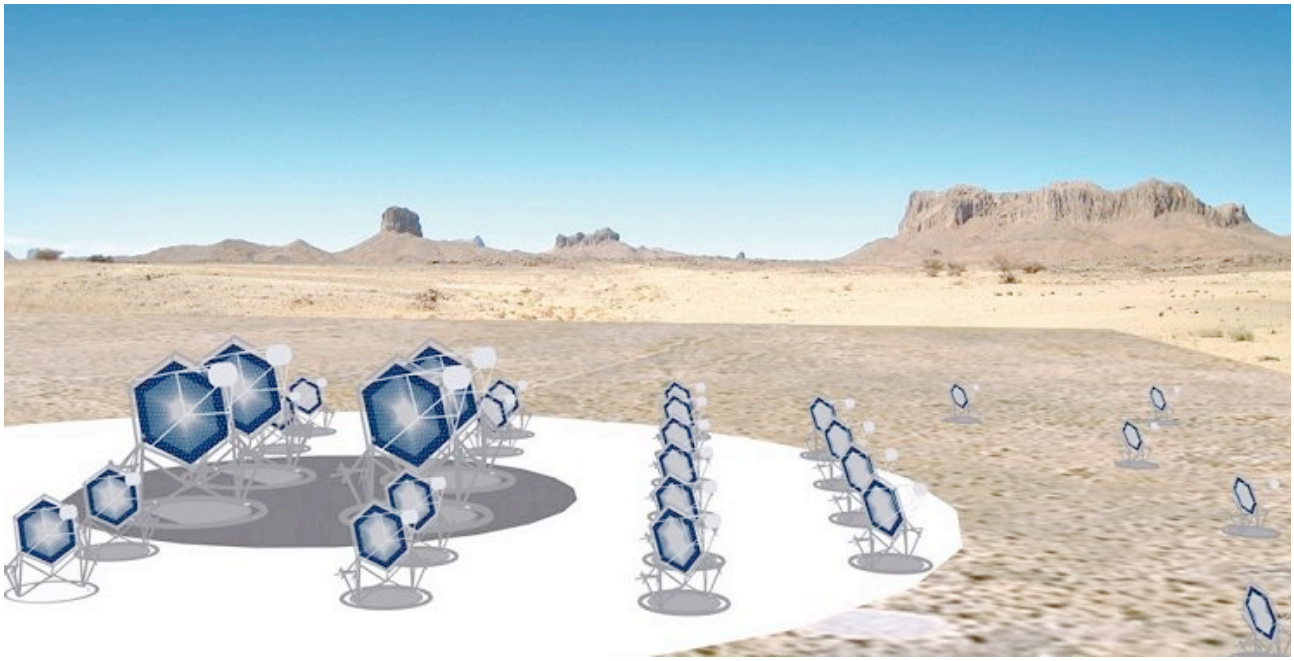

Prepared by:	Name:	R. Canestrari P. Conconi O. Catalano	Signature:		Date:	14-10-2011
Reviewed by:	Name:	S. Vercellone	Signature:		Date:	14-10-2011
Approved by:	Name:	G. Pareschi	Signature:		Date:	14-10-2011

TABLE OF CONTENTS

DISTRIBUTION LIST

ASTRI collaboration	astri@brera.inaf.it

DOCUMENT HISTORY

Version	Date	Modification
	14-10-2011	first version

LIST OF ACRONYMS

CTA	Cherenkov Telescope Array
DET	Detector
EC	Elemental Cell
M1	Primary Mirror
M2	Secondary Mirror
PDM	Photon Detection Module
SST	Small Size Telescope

APPLICABLE DOCUMENTS

[AD1]

REFERENCE DOCUMENTS

[RD1] 1

1. INTRODUCTION

This document describes the optical design for a wide filed, aplanatic, double-reflection Cherenkov telescope of 4 meters class.

This design is developed by INAF in the framework of the ASTRI project and it will be implemented into the end-to-end prototype to be developed. The proposed layout intends to be fully compliant with the requirements for the telescopes composing the SST array of the CTA Observatory.

The design hereafter presented is done taking into account both the segmentation of the primary mirror M1 shown in Figure 1.1 and the arrangement of detection units into the detector DET as shown in Figure 1.2 (a description of the detector arrangement and nomenclature is postponed in Section 4).

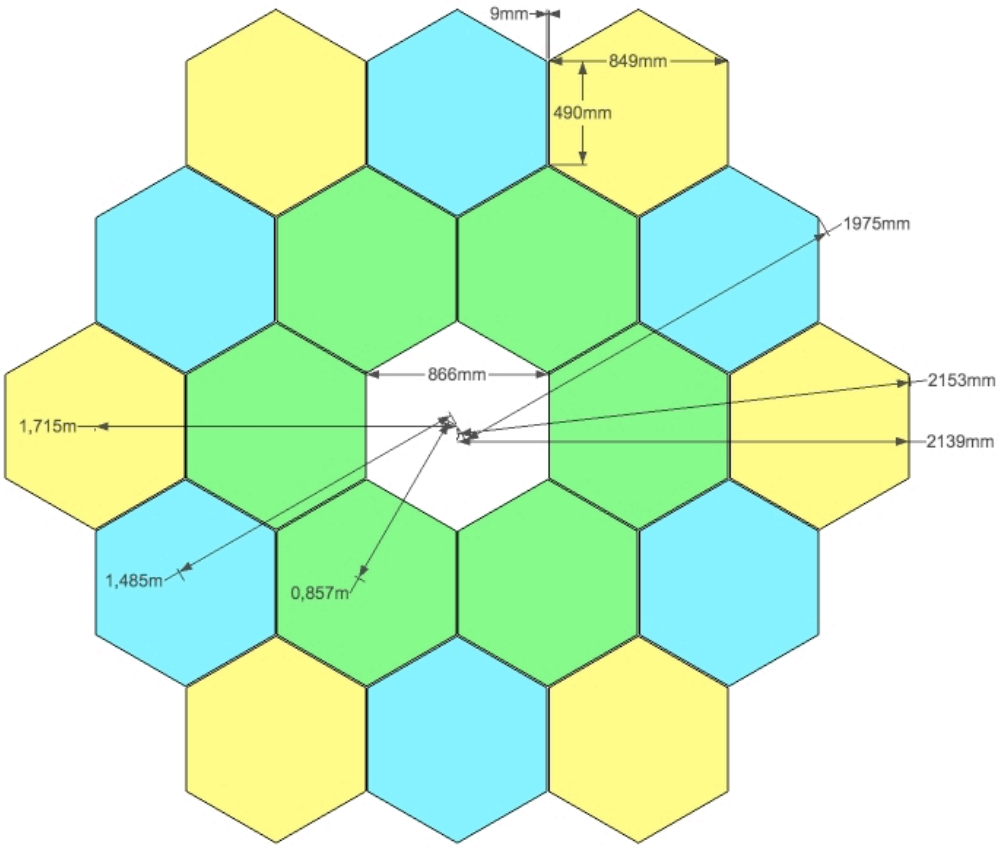

Figure 1.1 Tessellation of the primary mirror M1.

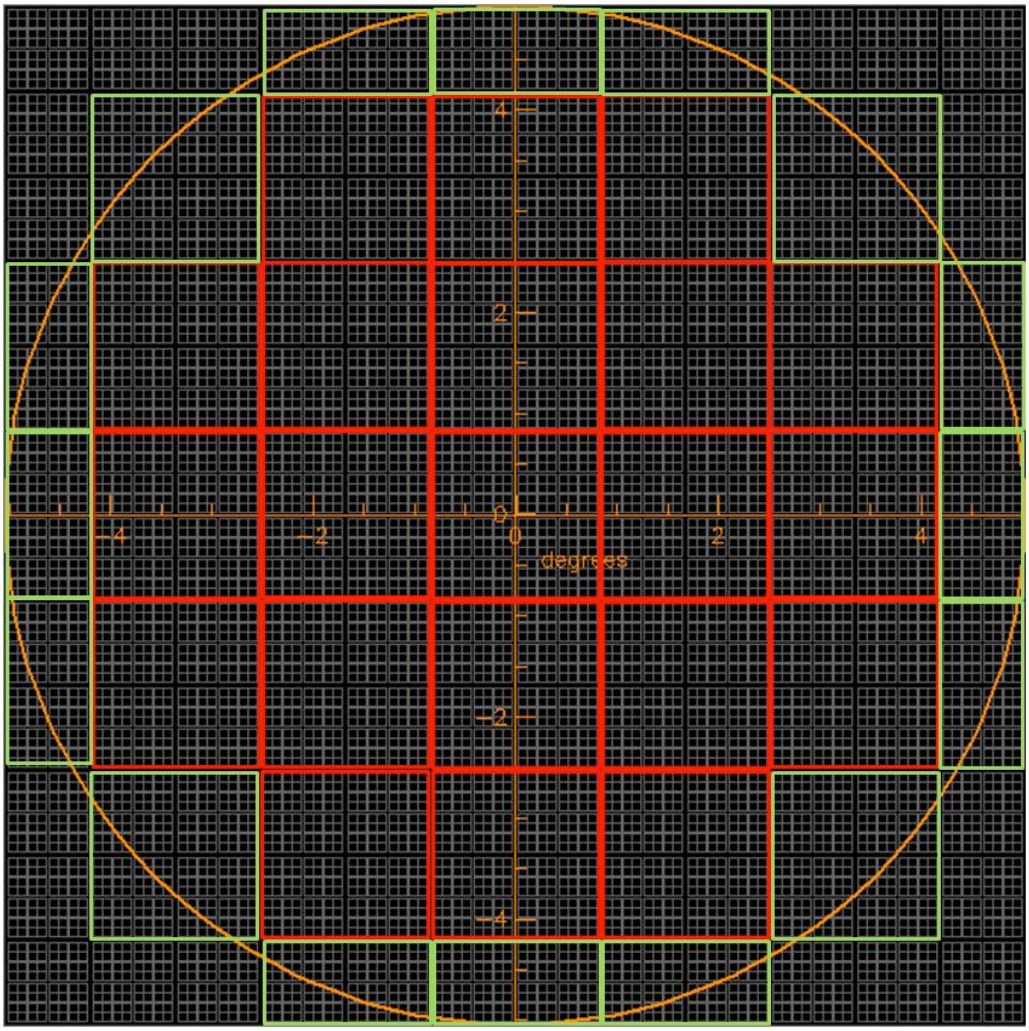

Figure 1.2 Arrangement of the detection units.

The design optimization has been done in such a way the amount of energy contained within 2x2 physical pixels, hereafter called *Cherenkov pixel*, is not less than 80% along the entire field angle. This parameter is named *Ensquared Energy*.

The design has been performed using the commercial software for optical system design ZEMAX.

2. THE OPTICAL LAYOUT

The optical system is a Schwarzschild-Couder configuration with a focal ratio F# of 0.5, see Figure 2.1. The design has plate scale of 37.5 mm/°, the Cherenkov pixel is approximately 0.16°, over an equivalent focal length of 2150 mm. This delivers a usable field of view up to 9.6° in diameter, the circle traced in Figure 1.2 encloses all the detection units and corresponds to the corrected field of view.

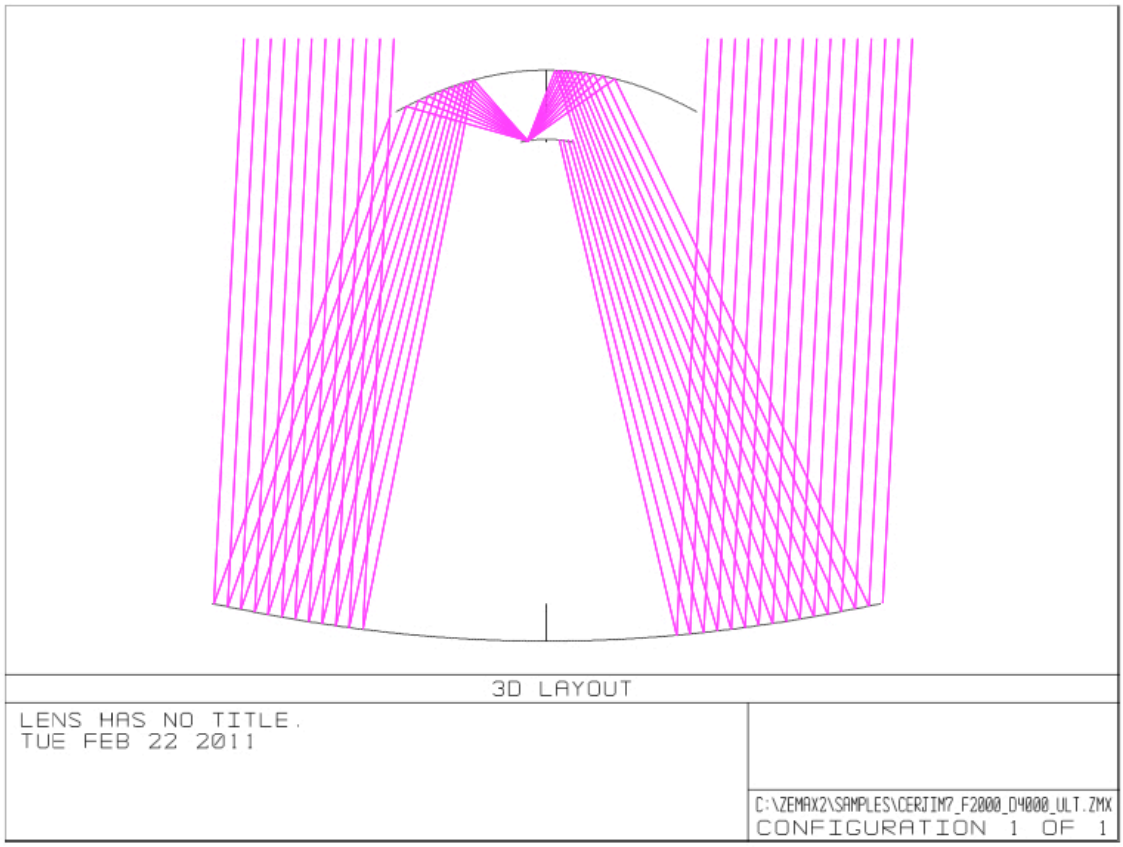

Figure 2.1 The Schwarzschild-Couder optical design adopted for ASTRI.

The images of a point source placed 10 km above the telescope are also shown. Figure 2.2 is a series of six zooms of the entire detector down to the Cherenkov pixel for the field angles: 0°, 1°, 2°, 3°, 4° and 4.8°. From these images have been evaluated the ensquared energies curves plotted in Figure 2.3.

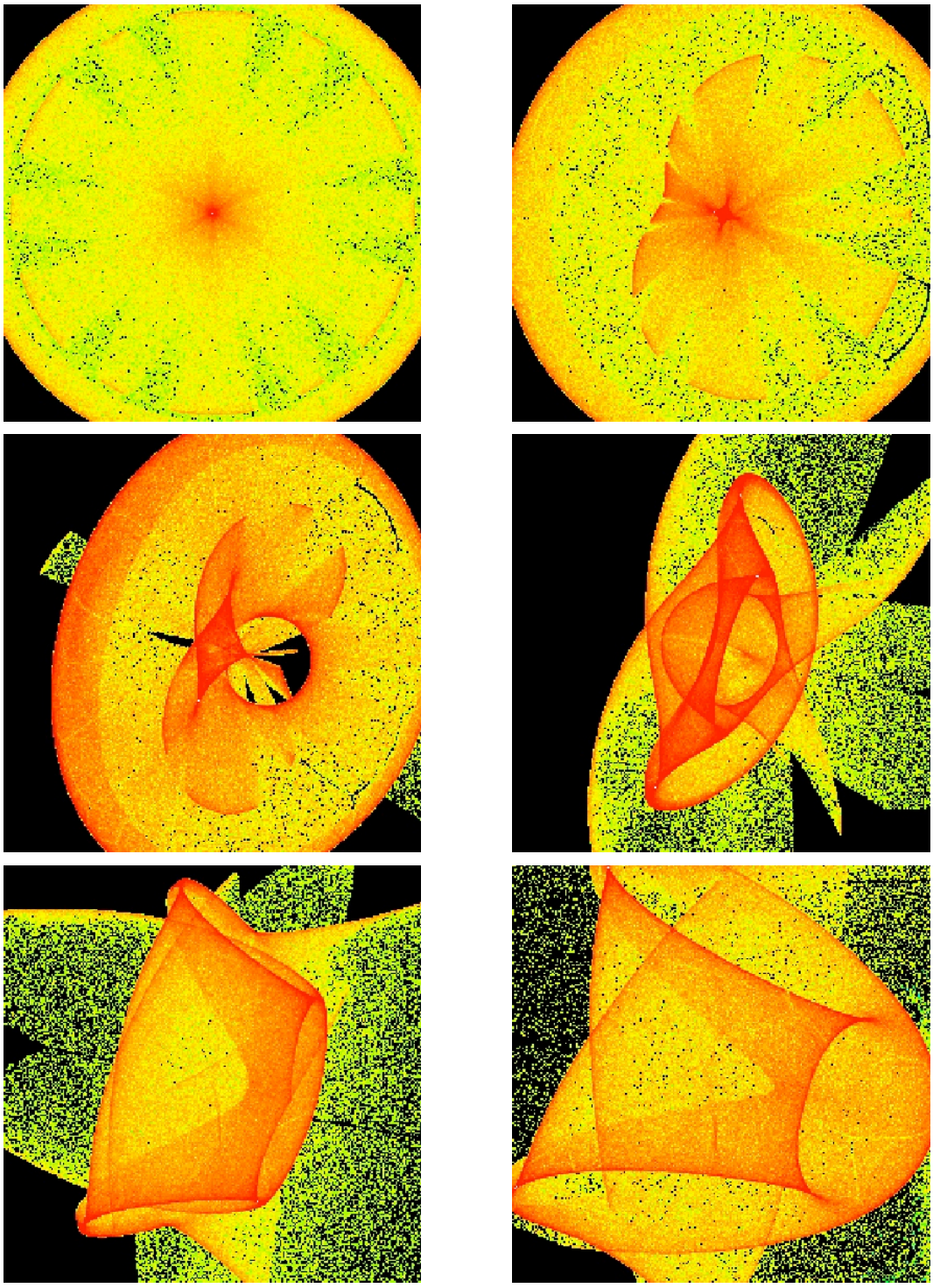

Figure 2.2 Images for 0°, 1°, 2°, 3°, 4° and 4.8° of field angle of a point source located 10 km above the telescope. The images are oversampled because each box has the same dimensions of a Cherenkov pixel.

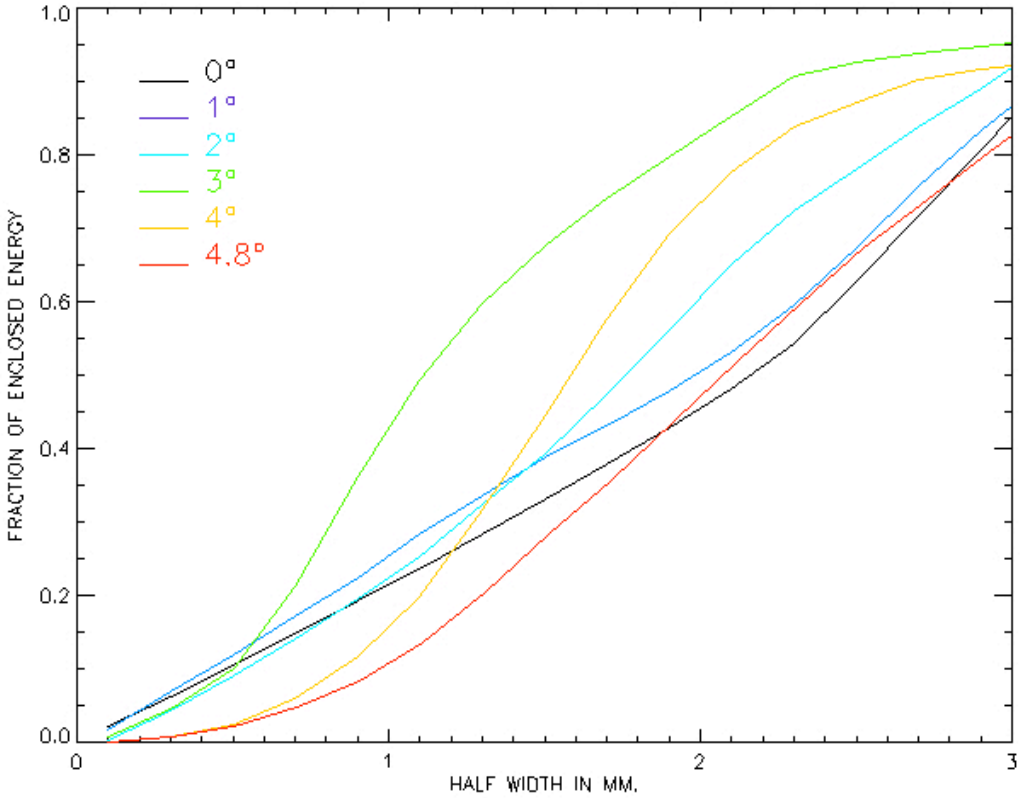

Figure 2.3 Ensquared energy for various field angles.

Concerning the throughput we give the effective area, expressed in squared meters, of the entire optical system taking into account:

- segmentation of the primary mirror;
- obscuration of the secondary mirror;
- obscuration of the detector;
- reflectivity of M1 and M2 (standard coated, mean reflectivity 90%) as function of the energy and incident angle;
- a protection window for the detector (standard coated, transmission > 98%);
- efficiency of the detector as function of the incident angles (ranging from 25° to 72°).

The values in Table 2.1 do not consider the quantum efficiency of the detector and the absorption from the atmosphere, whilst they are calculated as function of the incoming wavelengths (λ1=320nm; λ2=350nm; λ3=400nm; λ4=450nm; λ5=500nm; λ6=550nm; λ7=600nm) for different field angles.

To complete the optical design description we report also the temporal behavior of the optics. Figure 2.4 shows that the system is isochronous down to $3x10^{-12}$ s.

	A(λ1)	A(λ2)	A(λ3)	A(λ4)	A(λ5)	A(λ6)	A(λ7)
0°	6.30	6.38	6.41	6.56	6.69	6.76	6.75
1°	6.28	6.38	6.39	6.56	6.67	6.77	6.76
2°	6.26	6.35	6.38	6.50	6.61	6.72	6.66
3°	6.15	6.22	6.31	6.39	6.57	6.60	6.60
4°	5.86	5.98	6.03	6.13	6.28	6.27	6.38
4.8°	5.87	5.86	5.90	6.04	6.16	6.21	6.22

Table 2.1 Effective area of the entire optical system as described before.

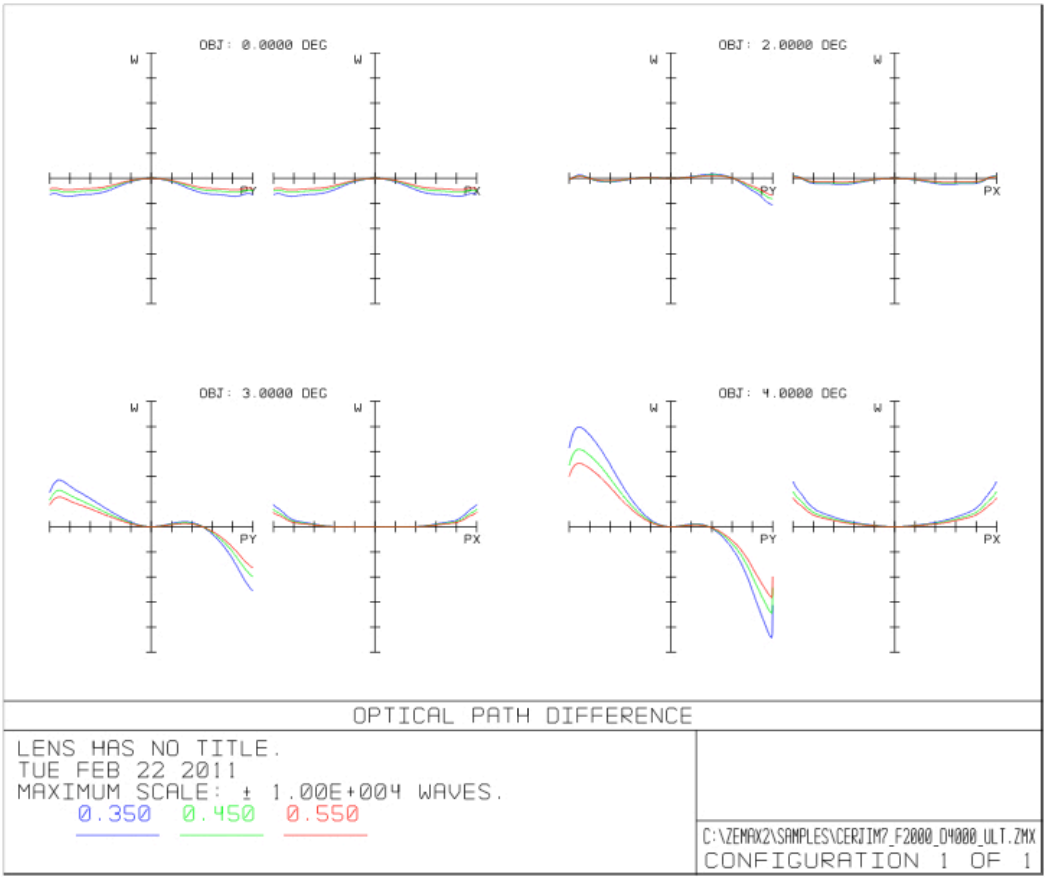

Figure 2.4 Temporal behavior of the optical system.

3. THE OPTICAL SURFACES

The mirror surfaces can be described with the following polynomial equation:

$$z = \frac{cr^2}{1+\sqrt{1-(1+k)c^2r^2}} + \sum_{i=1}^{N} \alpha_i r^{2i}$$

where z is the surface profile, r the surface radial coordinate, c the curvature (the reciprocal of the radius of curvature), k the conical constant, α_i the coefficients of the asphere.

The main system dimensions are listed in Table 3.1. Figure 3.1 shows the sags as a function of the surface radial coordinate for M1 and M2 respectively.

ELEMENT NAME	DIAMETER [mm]	RADIUS OF CURVATURE [mm]	SHAPE	DISTANCE TO... [mm]
M1	4306	-8223	Even asphere	M2: 3108.4
M2	1800	2180	Even asphere	DET: 519.6
DET	(side) 360	1000	--	--

Table 3.1 Optical system main dimensions.

3.1 The primary mirror, M1

The primary mirror is segmented following the scheme reported in Figure 1.1. The full reflector is composed of 18 segments (the central one is not used). The segmentation requires three types of segments having different surface profiles:

- the green segments, inner corona: M1a;
- the light blue segments, central corona: M1b;
- the yellow segments, outer corona: M1c.

The segments have hexagonal shape with aperture equal to 849 mm from face to face. Each segment has 9 mm of gap from the neighbors for mounting and alignment purposes. Each segment will be equipped with two actuators plus one fixed point for alignment. Only tilt misplacements will be corrected; piston correction will not be available for the primary mirror segments.

Adopting the same mathematical notation introduced before we report in Table 3.2 the description of the surface profile of M1.

COEFFICIENT	M1
α_1	0.00
α_2	9.61060e-013
α_3	-5.65501e-020
α_4	6.77984e-027
α_5	3.89558e-033
α_6	5.28038e-040
α_7	-2.99107e-047
α_8	-4.39153e-053
α_9	-6.17433e-060
α_{10}	2.73586e-066

Table 3.2 Coefficients describing the aspherical terms in M1.

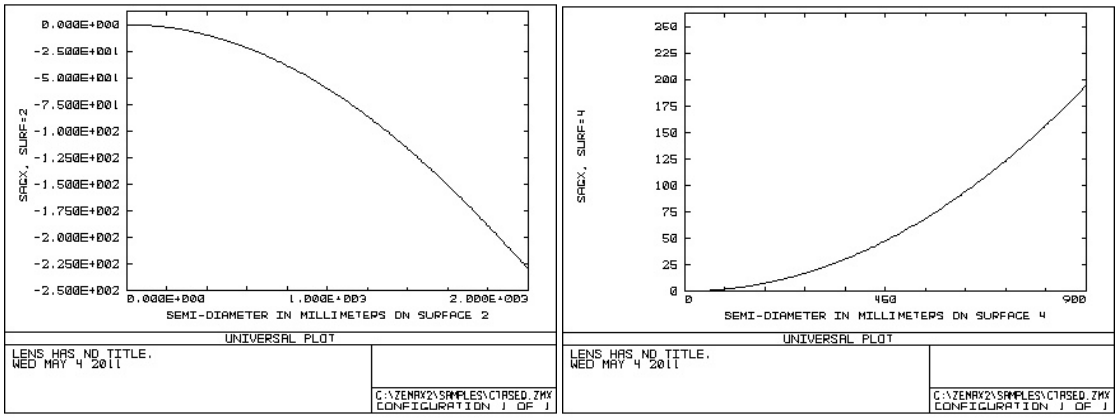

Figure 3.1 Sags of M1 (left) and M2 (right) as function of the surface radial coordinate.

3.2 The secondary mirror, M2

The secondary mirror is monolithic and equipped with three actuators. The implementation of the third actuator makes available also the piston/focus adjustment for the entire optical system.

Adopting the same mathematical notation introduced before we report in Table 3.2.1 the description of the surface profile of M2.

COEFFICIENT	M2
α_1	0.00
α_2	1.62076e-011
α_3	-2.89584e-017
α_4	8.63372e-024
α_5	3.34856e-030
α_6	-1.03361e-036
α_7	-6.73524e-043
α_8	-3.06547e-049
α_9	3.17161e-055
α_{10}	-3.71183e-062

Table 3.2.3 Coefficients describing the aspherical terms in M2.

4. THE DETECTOR ASSEMBLY

The detector is based on Silicon Photon Multiplier devices made up of APDs operated in Geiger mode. The design presented in this document makes use of devices available on the market and their arrangement is one constrain adopted for the trade-off.

Figure 4.1 shows the basic units and the way in which we intend to assemble them together:

- The UNIT is the primary monolithic device; it is composed of 4x4 pixels of 3 mm in side. A group of 2x2 pixels forms the Cherenkov pixel.
- The ELEMENTAL CELL EC is a symmetric assembly of 2x2 UNITs mounted on a PCB.
- The PHOTON DETECTION MODULE PDM is made up by 2x2 ECs for a total number of 256 pixels; it maintains a symmetry top-bottom and left-right; it is the basic detection unit to be mechanically integrated into the camera body. Over the geometrical area covered by one PDM, the dead area is about 31.5%.

This optical design delivers up to 9.6° of corrected field of view corresponding to a grid of 7x7 PDMs. The field of view can be filled with 31 PDMs (25 + 12 half PDMs) arranged as shown in Figure 1.2, the grand total of Cherenkov pixels will be 1984. In Table 4.1 are listed the *(x, y, z)* coordinates of the centers of each PDM and their *(x, y)* tilts.

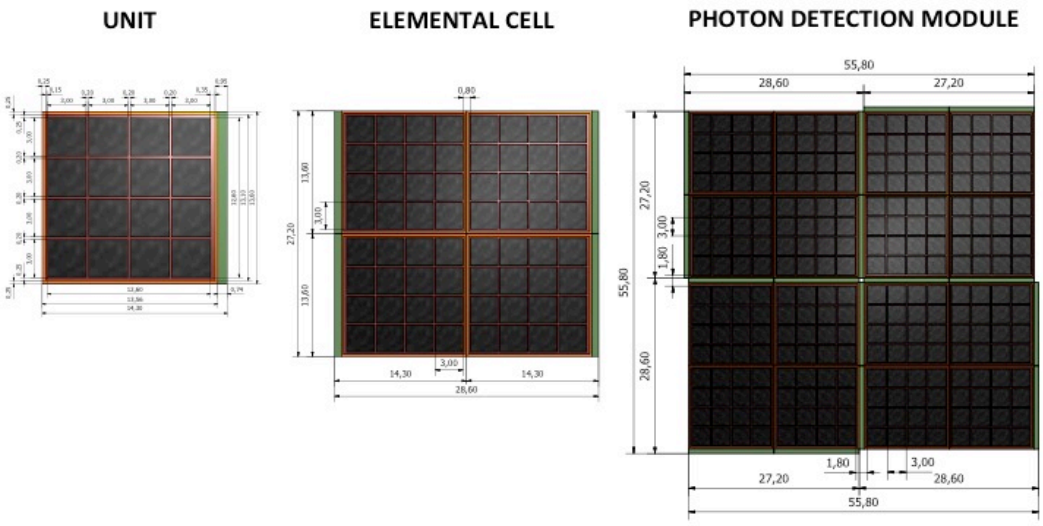

Figure 4.1 Adopted nomenclature of SiPM detection units.

Coordinates [mm]			Tilts [°]	
x	*y*	*z*	*x*	*y*
-159.76	-57.96	-13.66	-9	-3
-159.76	0.00	-12.14	-9	0
-159.76	57.96	-13.66	-9	3
-115.76	-115.76	-12.14	-6	-6
-115.76	-57.96	-7.58	-6	-3
-115.76	0.00	-6.07	-6	0
-115.76	57.96	-7.58	-6	3
-115.76	115.76	-12.14	-6	6
-57.96	-159.76	-13.66	-3	-9
-57.96	-115.76	-7.58	-3	-6
-57.96	-57.96	-3.04	-3	-3
-57.96	0.00	-1.52	-3	0
-57.96	57.96	-3.04	-3	3
-57.96	115.76	-7.58	-3	6
-57.96	159.76	-13.66	-3	9
0.00	-159.76	-12.14	0	-9
0.00	--115.76	-6.07	0	-6
0.00	-57.96	-1.52	0	-3
0.00	0.00	0.00	0	0
0.00	57.96	-1.52	0	3
0.00	115.76	-6.07	0	6
0.00	159.76	-12.14	0	9
57.96	-159.76	-13.66	3	-9
57.96	-115.76	-7.58	3	-6
57.96	-57.96	-3.04	3	-3
57.96	0.00	-1.52	3	0
57.96	57.96	-3.04	3	3
57.96	115.76	-7.58	3	6
57.96	159.76	-13.66	3	9

115.76	-115.76	-12.14	6	-6
115.76	-57.96	-7.58	6	-3
115.76	0.00	-6.07	6	0
115.76	57.96	-7.58	6	3
115.76	115.76	-12.14	6	6
159.76	-57.96	-13.66	9	-3
159.76	0.00	-12.14	9	0
159.76	57.96	-13.66	9	3

Table 4.1 Coordinates and tilts of the PDMs composing the detector assembly.

5. TOLERANCES

Tolerances are calculated in such a way the ensquared energy contained in one Cherenkov pixel does not drop below 70%.

The *(x, y)* displacements and tilts of M2 translate essentially in pointing errors. Displacements on *z* translate in defocusing: they can be fixed correcting the piston by adjustments of the three actuators. A similar consideration can be done for the detector, but keeping in mind that *δz* of M2 and *δz* of DET are not independent. For this reason we give both the constrain on the M1-DET distance and *δz* of M2 (expressed as the minimum stroke needed by the actuators to compensate the defocus).

The *(x, y)* displacements of M1 can be kept, in principle, wide as the 9 mm of gap between each segment (anti-collision), but they will result tighter by mechanical considerations on the supporting structure. The *z* displacement refers to the overall surface of the primary mirror, each segment respects to the other.

Figure 5.1 shows the image of a point source, for different field angles, generated from random misalignments of the optical components.

M1A,B,C	**δx [mm]**	**δy [mm]**	**δz [mm]**	**tx ['']**	**ty ['']**
	±2	±2	±1	±1	±1
M1-DET	**δx [mm]**	**δy [mm]**	**δz [mm]**	**tx ['']**	**ty ['']**
	--	--	±1	--	--
M2	**δx [mm]**	**δy [mm]**	**δz [mm]**	**tx ['']**	**ty ['']**
	±2	±2	±5	±3	±3

Other relevant tolerances concern the shape deviation errors and microroughness tolerable on the mirrors surfaces.

Concerning the microroughness, it scatters the light causing the blurring of the PSF and the increase of the background light on adjacent pixels. The microroughness is evaluated for spatial frequencies below the millimeter scale; the maximum tolerable value is 4-5 nm rms.

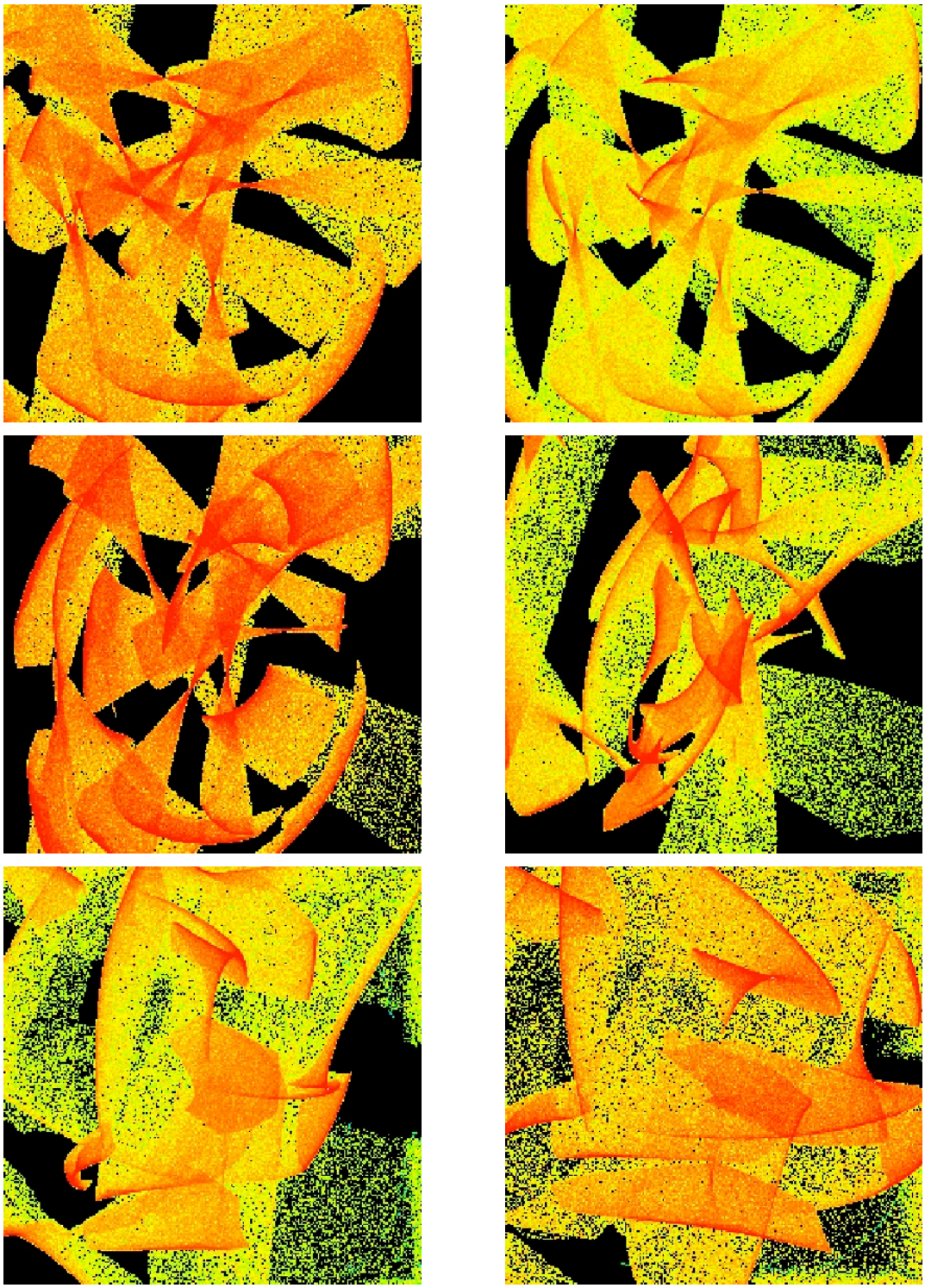

Figure 0.1 Images for 0°, 1°, 2°, 3°, 4° and 4.8° of field angle of a point source located 10 km above the telescope generated by random misalignments. The images are oversampled because each box has the same dimensions of a Cherenkov pixel.

6. FEATURED ENHANCEMENTS

The optical design and its performances as they are depicted in the previous sections of this document shall to be considered the baseline choice for the ASTRI prototype. It can be implemented exactly as described before; we call it *naked configuration*, i.e. without requiring any particular technological development (apart from the obvious work needed for the mirrors and detector implementations). The naked configuration provides a sort of minimum performances at the minimum cost; performances that are in any case already compliant with the main needs of CTA.

In this section, some enhancements are described in order to push these performances. These enhancements can be effective only subsequently to their technological developments. Table 6.1 shows the ideal effective area achievable in case of total reflection or transmission of the optical components.

	A(λ1)	A(λ2)	A(λ3)	A(λ4)	A(λ5)	A(λ6)	A(λ7)
0°	6.55	7.24	7.38	7.46	7.46	7.35	7.08
1°	6.53	7.24	7.36	7.46	7.44	7.36	7.09
2°	6.51	7.20	7.35	7.39	7.37	7.31	7.00
3°	6.40	7.05	7.27	7.28	7.33	7.18	6.93
4°	6.09	6.79	6.95	6.97	7.00	6.82	6.70
4.8°	6.10	6.65	6.80	6.87	6.98	6.75	6.53

Table 6.1 Effective area of the optical system equipped with the described enhancements.

6.1 Reimaging system

The reimaging system has the aim to recover the losses caused by photons that go into the detector dead area. Depending from its implementation, it will be possible to recover up to the 70% of photons losses.

As example, placing a sort of truncated pyramid having the smaller base equal to the detection-active dimension of the UNIT in front of each of them, it is easy to recover the majority of the photons losses apart from the 12% that falls between the individual pixels. Figure 6.1.1 shows the concept just described. Moreover, using a proper glass type with the index of refraction as high as possible and with good transmission in the desired energy band, it is possible to limit the thickness of those pyramids to few millimeters. A reimaging system like this actually acts also as the protection window.

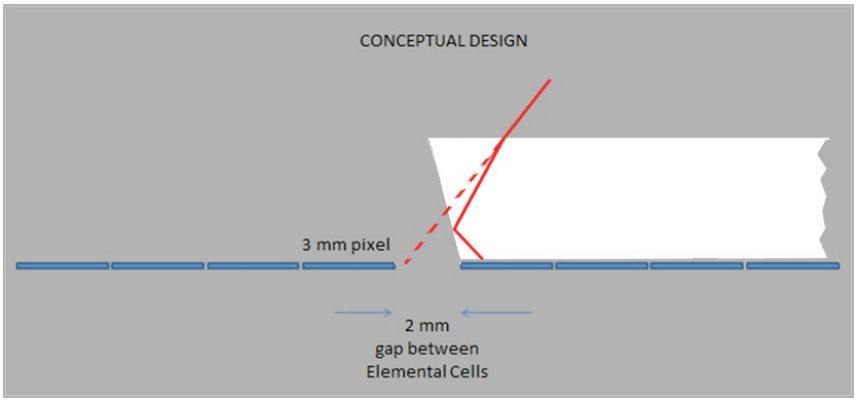

Figure 6.1.1 Conceptual design of the reimaging system (the drawing is not in scale).

6.2 Coatings

Coatings are very important for the optical systems. In this case, a fraction of the effective area as large as the 12-15% of that of the naked configuration can be gained simply using proper coatings. As an example, we report in Figure 6.2.1 two reflectivity curves related to a standard coating (Aluminum plus Quartz) and a multilayer coating.

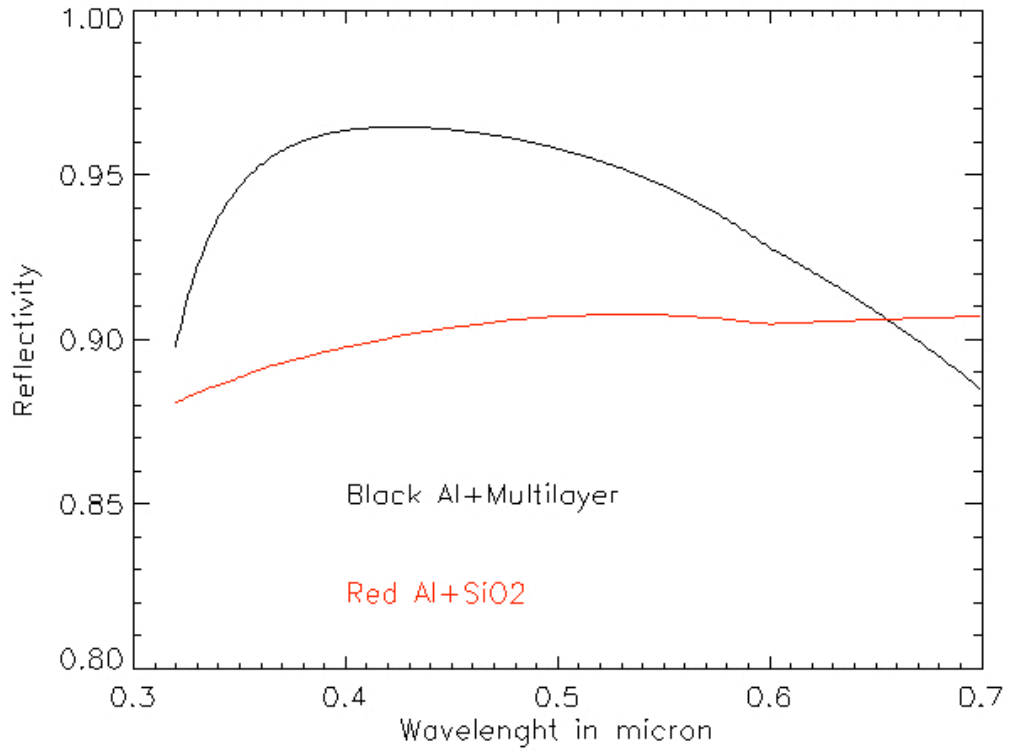

Figure 6.2.1 Comparison between possible coatings for enhancing the reflectivity of the mirrors.

6.3 Baffle

In the Schwarzschild-Couder layout the detector is facing the sky all the time. A proper baffle can be applied during the telescope observation mode in order to limit the amount of night sky background reaching the detector. For example, a cylinder properly sized (i.e. having the diameter of M2 and length as the distance M2-DET) can act as desired, see Figure 6.3.1.

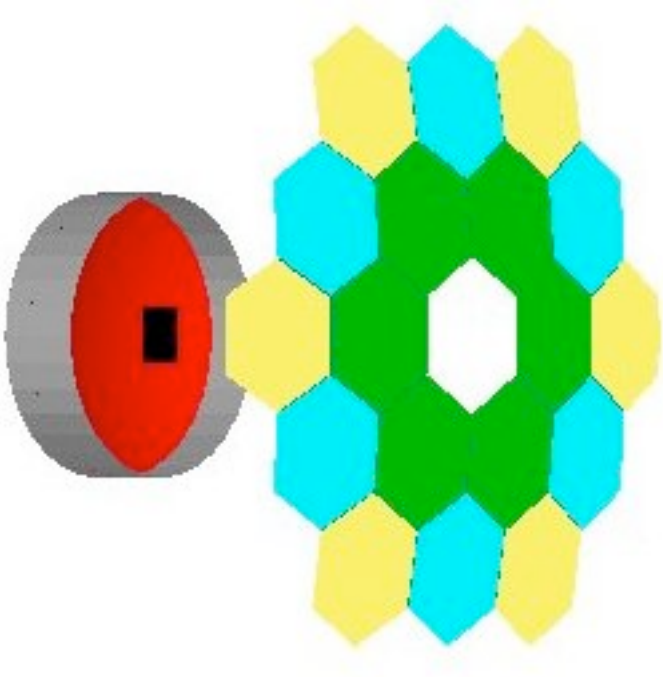

Figure 6.3.1 Drawing of the baffle concept. The black rectangle represents the detector, the red circle is M2 and the grey cylinder is the baffle.